COMPACT TRIPLE-BAND BANDPASS FILTER USING MULTI-MODE RESONATOR (MMR) WITH MULTIPLE TRANSMISSION ZEROS

Xuebin TANG and Shuping JIN

Changzhou Institute of Mechatronic Technology, Changzhou, 213164, China.

tang_xue_bin@163.com, jinshuping@126.com

Abstract: *In this article, a compact triple-band microstrip bandpass filter (BPF) with tunable centre frequencies and bandwidths as well as multiple transmission zeros (TZs) is presented. The proposed filter is designed based on a novel multi-mode resonator (MMR), and the even-/odd-mode analysis method is employed to investigate its resonant characteristics. By changing the lengths of two loaded coupled open stubs and coupling space between them, two resonant modes can be tuned and the bandwidth can be controlled. Also, two additional TZs are generated due to the dual-finger feed structure. Moreover, these two TZs can be controlled by the lengths of two fingers, and high passband selectivity and band-to-band isolation level are achieved with ten TZs. The three centre frequencies of the proposed triple-band BPF are located at 1.9, 3.55, and 7.33 GHz, respectively. In addition, the overall circuit size of the fabricated filter is much smaller in comparison with previous works. For demonstration, a prototype filter is fabricated and measured, and good agreements are obtained between the measured results and electromagnetic (EM) simulated ones.*

Keywords: *Bandpass filter (BPF), multi-mode resonator (MMR), transmission zeros, triple-band filter.*

1. Introduction

In modern wireless communication systems, multi-service technology has been widely and aggressively developed. Thus, as an important circuit block, multi-band planar bandpass filters (BPFs) have gained a lot of attention over past few years. Extensive efforts have been made to design multi-band BPFs, and various literatures about multi-band filters have been reported [1-19]. Quarter-wavelength resonators [1-3] have been employed to construct dual-band or tri-band BPFs. In [4], and [5], tri-section stepped-impedance resonators (SIRs) are utilized to design triple-band filters. However, the insertion losses need to be improved and the circuit sizes are comparatively large. Shorted-ended SIRs [6], [7] have been used to realize dual- and triple-band BPFs, whereas asymmetric SIRs are introduced to design triple-band BPFs with compact size in literatures [8], and [9]. Stub-loaded resonators (SLRs) [10-12] and square ring loaded resonators (SRLRs) [13], [14] are also proved to be capable of designing triple-band filters. Recently, the design method to achieve high performance multi-band BPFs utilizing multi-mode resonators (MMRs) has been attracting much more attention [15-19]. However, there is still much research work to do to design filters with compact circuit size and high skirt selectivity and

band-to-band isolation level with multiple transmission zeros (TZs).

This paper presents a compact triple-band BPF using a novel MMR. The proposed MMR is symmetric in structure, and the even-/odd-mode analysis method is employed to investigate its resonant characteristics. By properly tuning the design parameters, the resonant frequencies can be freely chosen. In addition, by changing the lengths of two loaded coupled open stubs and coupling space between them, two resonant modes can be tuned and the bandwidths can be controlled. Also, two additional TZs are generated due to the dual-finger feed structure and can be controlled by the lengths of two fingers. Thus, high passband selectivity and band-to-band isolation level are obtained with nine TZs. In order to validate the design method, a triple-band filter centred at 1.9/3.55/7.33 GHz with 3-dB fractional bandwidths (FBWs) of 14.2/7.9/11.6% is simulated and fabricated. The simulation works of the prototype filter are performed by using a commercial electromagnetic (EM) simulator IE3D, and the measured results show good agreement with the simulated ones.

2. Analysis of the Proposed MMR

Fig. 1(a) shows the specific geometrical schematic of the proposed MMR. It is mainly constructed by a meandered square-loop loaded with a pair of coupled open
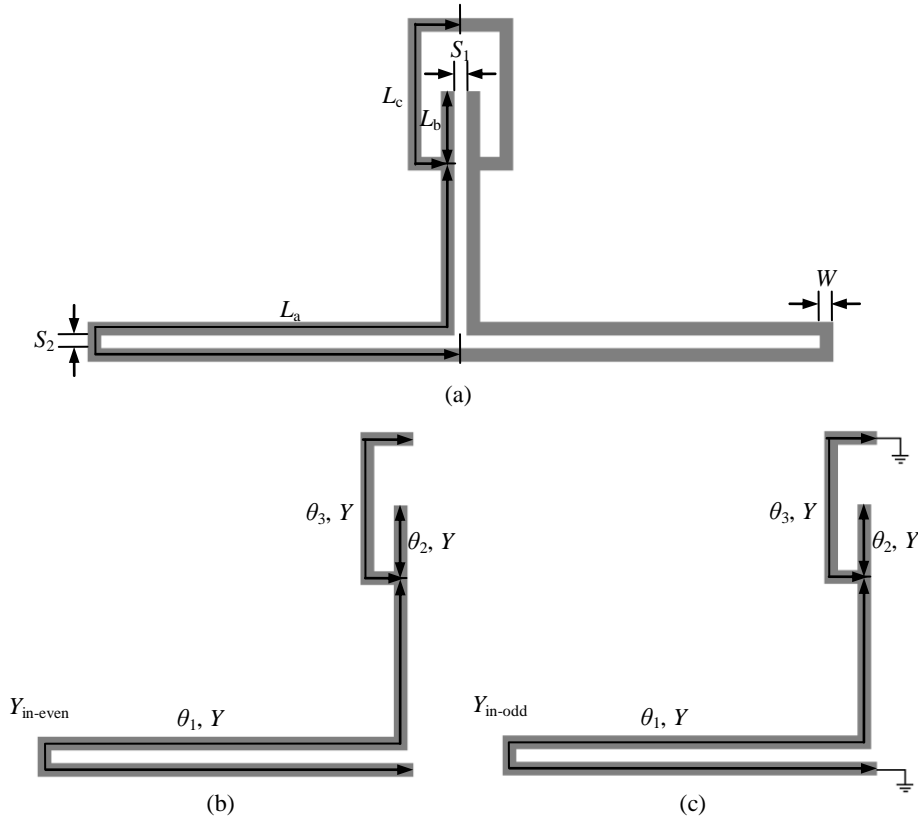
Fig. 1. (a) Specific geometrical schematic of the proposed MMR. (b) Even- and (c) odd-mode equivalent circuits.

stubs. Since the proposed MMR is symmetrical in structure, the even-/odd-mode analysis method can be adopted to analyze its resonant characteristics. Its even- and odd-mode equivalent circuits are illustrated in Figs. 1(b) and (c), respectively. The microstrip lines with electrical lengths of θ_1, θ_2, and θ_3 have the same admittance of Y. Thus, the input admittances of the even- and odd-mode equivalent circuits can be found as follows

$$Y_{in-even} = jY\frac{\tan\theta_1 + \tan\theta_2 + \tan\theta_3}{1 - \tan\theta_1(\tan\theta_2 + \tan\theta_3)}$$

(1)

$$Y_{in-odd} = -jY\frac{\tan\theta_1 + \tan\theta_2 - \cot\theta_3}{\tan\theta_1(\tan\theta_2 - \cot\theta_3) - 1}$$

(2)

The even-mode resonance occurs under the condition of $Y_{in\text{-}even} = 0$, and the odd-mode resonance occurs when $Y_{in\text{-}odd} = 0$, that is

$$\tan\theta_1 + \tan\theta_2 + \tan\theta_3 = 0 \quad \text{for even mode}$$

(3)

$$\tan\theta_1 + \tan\theta_2 - \cot\theta_3 = 0 \quad \text{for odd mode}$$

(4)

From Figs. 1(b), and (c), one can clearly observe that there are four different resonant sections of the proposed MMR, i.e., the sections with lengths of $L_a + L_b$ and $L_a + L_c$ in even- and odd-mode equivalent circuits. Therefore, the even- and odd-mode resonant frequencies, $f_{even1}, f_{even2}, f_{odd1},$ and f_{odd2}, generated by the

four resonant sections can be approximately estimated by equations (5) - (8) [8] as

$$f_{even1} \approx \frac{nc}{2(L_a + L_b)\sqrt{\varepsilon_{eff}}} \qquad n = 1, 2, 3, \ldots\ldots \quad (5)$$

$$f_{even2} \approx \frac{nc}{2(L_a + L_c)\sqrt{\varepsilon_{eff}}} \qquad n = 1, 2, 3, \ldots\ldots \quad (6)$$

$$f_{odd1} \approx \frac{nc}{4(L_a + L_b)\sqrt{\varepsilon_{eff}}} \qquad n = 1, 3, 5, \ldots\ldots \quad (7)$$

$$f_{odd2} = f_{even2} \qquad\qquad\qquad\qquad\qquad (8)$$

where f_{even1} and f_{odd1} are the even- and odd-mode resonant frequencies generated by the resonant section with length of $L_a + L_b$, and f_{even2} and f_{odd2} are the even- and odd-mode resonant frequencies created by the $L_a + L_c$ section, respectively. The number n denotes the nth spurious resonant frequency and

$$\varepsilon_{eff} = \frac{\varepsilon_r + 1}{2} + \frac{\varepsilon_r - 1}{2}\left[\left(1 + 12\frac{h}{w}\right)^{-0.5} + 0.04\left(1 - \frac{w}{h}\right)^2\right] \quad (9)$$

is the effective dielectric constant, where ε_r and h denote the relative dielectric constant and thickness of the substrate, respectively. Thus, desired resonant frequencies can be obtained by properly selecting the design parameters according to equations (5) - (8).

Figs. 2(a) and 2(b) depicts the resonant characteristics of the proposed MMR under weak coupling with varied L_b and S_1. Fig. 2(a) reveals that f_{odd1} and f_{odd2} decrease with the increase of L_b, whereas $f_{even1}, f_{even2},$ and f_{even3} remain constant. This conclusion can also be observed from equations (5) - (8). Moreover, it can be observed from these

two plots that, the second passband formed by f_{odd1} and f_{even2} can be easily tuned by controlling the coupling strength between the two loaded coupled open stubs which is determined by the value of L_b and S_1.
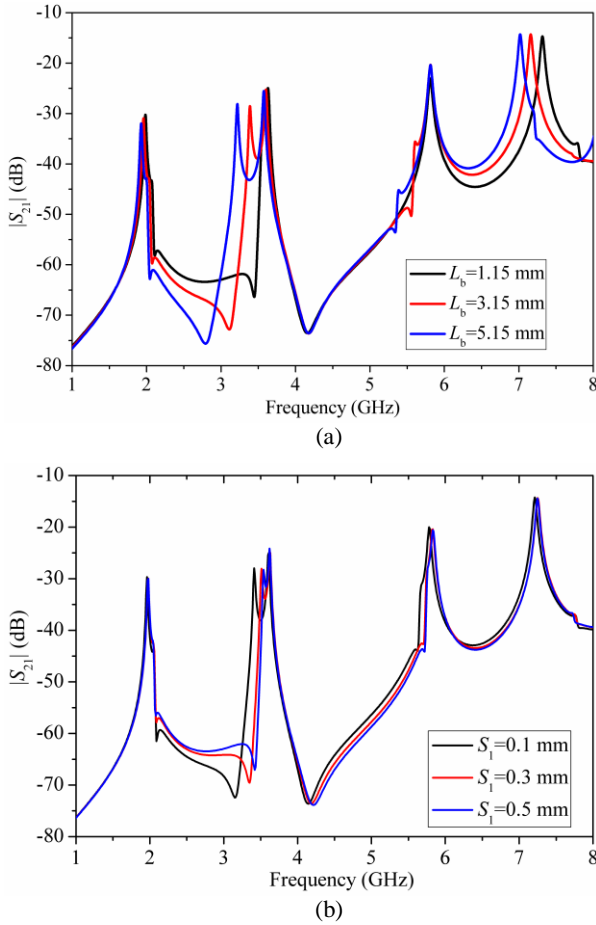
Fig. 2. Simulated $|S_{21}|$ of the proposed MMR under weak coupling with varied (a) L_b, and (b) S_1.

3. Analysis of Transmission Zeros
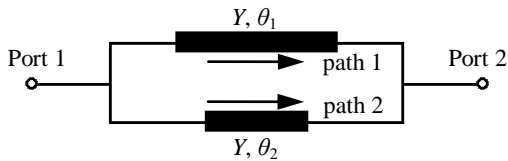
Fig. 3. Transversal signal interference model of the proposed BPF.

As shown in Fig. 5, ten TZs are created in the frequency responses which improve the passband selectivity significantly. Among these TZs, TZ_1 and TZ_9 are inherent TZs of the proposed MMR as can be seen from Fig. 2. TZ_4 and TZ_6 are generated due to the loaded coupled lines. By changing the coupling length and gap between the two open stubs, i.e., the coupling strength between them, these two TZs can be tuned. As demonstrated in Figs. 2(a) and 2(b), TZ_4 and TZ_6 decrease with the increase of L_b and the decrease of S_1, i.e., these two TZs decrease with the increase of coupling strength between the two loaded coupled open

stubs. In addition, TZ_2, TZ_3, TZ_7, and TZ_8 are introduced by the dual-finger feed scheme. These four TZs decrease with the increase of lengths of the two fingers.

Among these ten TZs, TZ_5 is generated by the transversal signal interference effect [20]. As can be observed from Fig. 4, there are two different transmission paths for signals to transmit from port 1 to port 2, i.e., the upper path 1 and the lower path 2. Its transversal signal interference model is shown in Fig. 3. The characteristic admittance of the two transmission paths are the same as Y, and electrical lengths of θ_1 and θ_2, respectively. The transmission zeros occur under the following condition:

$$\theta_1 - \theta_2 = (2n+1)\cdot \pi \quad \text{at } f_{\text{TZ}} \quad n = 0, 1, 2, \ldots\ldots \quad (10)$$

where f_{TZ} denotes the transmission zero frequency. That means the difference between the electrical lengths of two transmission paths equals odd multiple of π. Thus, the phases of the two signals transmit from port 1 to port 2 through path 1 and path 2 are inverted at port 2, which results in out-of-phase cancellation and TZs are generated. In this work, TZ_5 is the case of $n = 0$.

4. Design Procedure

After the resonant characteristics of the proposed MMR is clear, the triple-band BPF can be designed accordingly. The specific configuration of the proposed triple-band BPF is shown in Fig. 4. This filter is mainly constructed by the proposed MMR discussed in the last section. By meandering the L_a section in Fig. 1(a) and using a dual-finger feed structure with source-load coupling, the triple-band filter is obtained.

Fig. 5 demonstrates the simulated insertion losses of the proposed triple-band filter with the variation of L_9. One can clearly observe that the value of L_9 affects coupling strength of the third passband without influencing the first and second passbands. The parameter L_9 is selected as 8.1 mm after EM simulation and optimization (IE3D in this work) to obtained the desired coupling strength of the third passband. Also, the spurious frequencies at about 5.65 and 5.81 GHz are suppressed due to the decrease of the TZ introduced by the finger $L_8 + L_9$.

Thus, the design procedure is listed as the following steps. Firstly, the length $L_a + L_c$ is determined by the centre frequency of the first passband (f_1), and its value can be calculated from equation (6). Secondly, the initial length of L_b can be obtained with reference to equation (7). Then, tune the value of L_b and S_1 to achieve the desired bandwidth of the second passband. At last, the lengths of two fingers of the dual-finger feed structure, i.e., $L_8 + L_9$ and $L_{10} + L_{11}$, are tuned to obtain desired coupling strength to form the three passbands, and to generate two TZs at desired frequencies. These two TZs introduced by the two fingers are located at the frequencies where the physical lengths of the corresponding finger is equal to quarter-wavelength.

5. Results

In order to demonstrate the validity of the above-mentioned design method, the proposed triple-band BPF is designed and fabricated on a Rogers Duroid 4003 substrate with a thickness of 0.508 mm, a dielectric

constant ε_r of 3.55, and a loss tangent of 0.0027. The layout of designed filter is shown in Fig. 3. The

simulation works are carried out by the full-wave EM
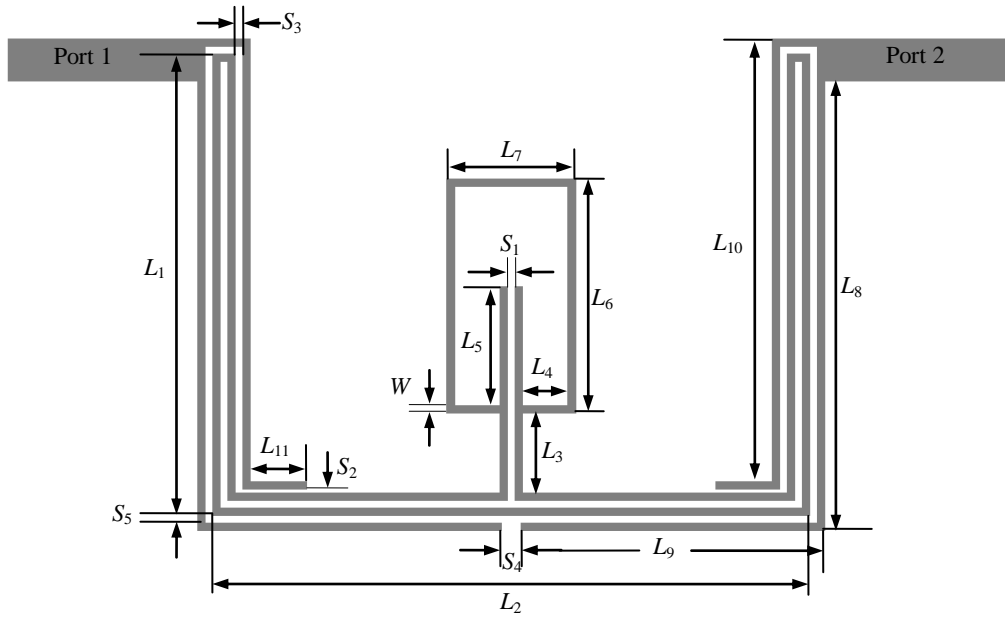
Fig. 4. Specific configuration of the proposed triple-band BPF. ($W = 0.2$ mm, $L_1 = 12.2$ mm, $L_2 = 15.8$ mm, $L_3 = 2.1$ mm, $L_4 = 1.2$ mm, $L_5 = 2.1$ mm, $L_6 = 6.2$ mm, $L_7 = 3.4$ mm, $L_8 = 11.89$ mm, $L_9 = 8.1$ mm, $L_{10} = 11.7$ mm, $L_{11} = 1.5$ mm, $S_1 = S_2 = S_5 = 0.1$ mm, $S_3 = 0.2$ mm, $S_4 = 0.5$ mm).
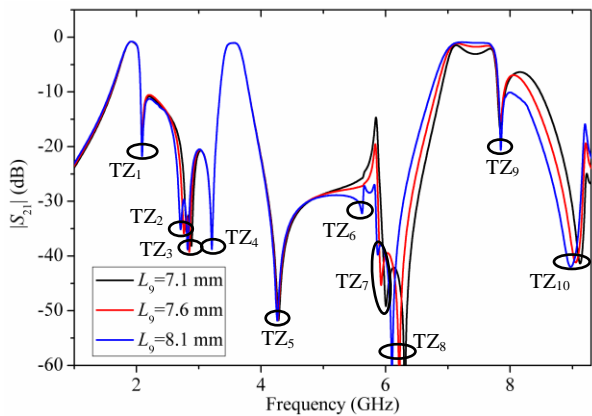
Fig. 5. Simulated $|S_{21}|$ of the proposed triple-band BPF with varied L_9.
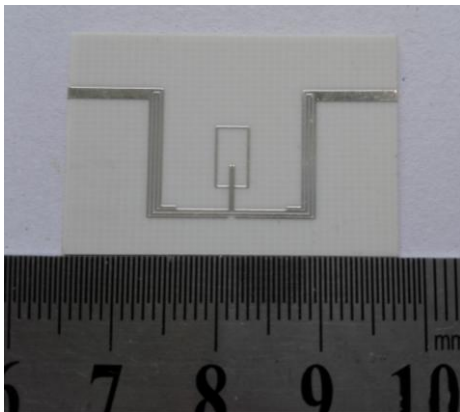
Fig. 6. Photograph of the fabricated triple-band filter.

simulator IE3D, and the measurements are performed with an Agilent's N5244A network analyzer.

Based on the design method described above, the structural parameters are obtained as follows: $W = 0.2$ mm, $L_1 = 12.2$ mm, $L_2 = 15.8$ mm, $L_3 = 2.1$ mm, $L_4 =$
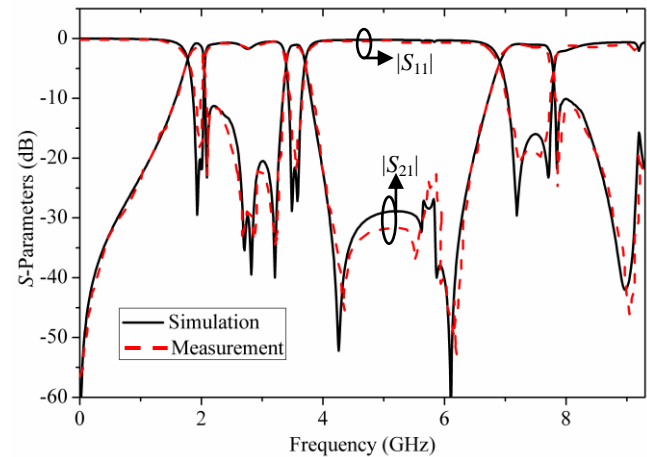
Fig. 7. Simulated and measured results of the designed triple-band filter.

1.2 mm, $L_5 = 2.1$ mm, $L_6 = 6.2$ mm, $L_7 = 3.4$ mm, $L_8 = 11.89$ mm, $L_9 = 8.1$ mm, $L_{10} = 11.7$ mm, $L_{11} = 1.5$ mm, $S_1 = S_2 = S_5 = 0.1$ mm, $S_3 = 0.2$ mm, $S_4 = 0.5$ mm. The overall circuit size occupies only 12.2 mm × 15.8 mm, i.e., approximately $0.123 \lambda_g \times 0.159 \lambda_g$, where λ_g is the guided wavelength at the center frequency of the first passband (1.9 GHz). Obviously, the proposed triple-band BPF is very compact in size.

The photograph of the fabricated prototype triple-band filter is shown in Fig. 6, and Fig. 7 plots the simulated and measured results of fabricated prototype filter. From Fig. 7, it can be observed that the measured and simulated results are in good agreement with each other. The measured center frequencies (CFs) of the fabricated triple-band filter

are 1.9/3.55/7.33 GHz, with the measured 3-dB FBWs of 14.2/7.9/11.6%, the minimum insertion losses (IL: $|S_{21}|$) of 0.86/1.1/1.23 dB and the return losses (RL: $|S_{11}|$)

better than 18/20/17 dB, respectively. It is worth mentioning that, ten TZs are generated at about 2.1, 2.63, 2.85, 3.2, 4.4, 5.51,

Table 1. Comparison of the proposed filter with other reported triple-band filters.

Refs.	CFs (GHz)	IL (dB)	RL (dB)	FBW (%)	TZ	Circuit Size ($\lambda_g \times \lambda_g$)
[2]	1.8/3.5/5.8	0.88/1.33/1.77	21.3/15.8/15.7	7/5/3.5	7	0.108 × 0.521
[4]	1/2.4/3.6	2/1.9/1.7	14/16/20	N/A	0	0.191 × 0.191
[7]	1.57/3.9/7	2/2.1/1.8	22/16/18	4.1/2/3	6	0.113 × 0.145
[9]	2.49/3.6/5.62	1.83/2.95/2.41	12/10/22	9.5/5.3/7.5	3	0.185 × 0.487
[11]	2.45/3.5/5.2	1.2/1.5/1.6	16.3/17.9/12.9	9.6/13.1/7.9	4	0.18 × 0.27
[13]	2.4/3.5/5.2	1.57/1.6/1.77	15/15/20	8.6/7.8/4.9	0	N/A
This work	1.9/3.55/7.33	0.86/1.1/1.23	18/20/17	14.2/7.9/11.6	10	0.123 × 0.159

(TZ denotes the number of transmission zeros.)

5.93, 6.2, 7.8 and 9 GHz, which improve the band-to-band isolation level and passband selectivity significantly. The comparison of the proposed filter with other reported triple-band filters is tabulated in Table 1. It can be observed that, the proposed triple-band BPF exhibits excellent performances of compact size, multiple transmission zeros, high skirt selectivity, low insertion loss, and high band-to-band isolation level.

6. Conclusion

In this paper, a compact triple-band microstrip BPF using a novel MMR with multiple TZs is presented. The proposed MMR is analyzed by even-/odd-mode analysis method to investigate its resonant characteristics. Then, a prototype triple-band BPF is designed, fabricated, and measured. Good agreement was obtained between the simulated and measured results. By properly tuning the design parameters, the resonant frequencies can be freely chosen. In addition, by changing the lengths of two loaded coupled open stubs and coupling space between them, two resonant modes can be tuned and the bandwidth of second passband can be controlled. Moreover, ten TZs are generated due to dual-finger feed structure, source-load coupling, transversal signal interference effect, and loaded coupled open stubs, which improves the band-to-band isolation level and passband selectivity greatly. The proposed compact triple-band filter is actually suitable for multi-band and multi-service applications in modern wireless communication systems.

7. References

[1] Zhang Songbai and Lei Zhu, "Compact Split-Type Dual-Band Bandpass Filter Based on λ/4 Resonators", *IEEE Microw. Wireless Compon. Lett.*, vol. 23, no. 7, pp. 344-346, Jul., 2013.

[2] Songbai Zhang and Lei Zhu, "Compact Tri-Band Bandpass Filter Based on λ/4 Resonators With U-Folded Coupled-Line", *IEEE Microw. Wireless Compon. Lett.*, vol. 23, no. 5, pp. 258-260, May, 2013.

[3] Jun Li, Shanshan Huang, Hui Wang, Yao Li, and Jianzhong Zhao, "A Novel Compact Tri-Band Bandpass Filter Using SIR Embedded Quarter-Wavelength Resonators", *Microw. Opt. Technl. Leet.*, vol. 57, no. 6, pp. 1345-1349, June 2015.

[4] Q. -X. Chu and X. -M. Lin, "Advanced Triple-Band Bandpass Filter Using Tri-Section SIR", *Electron. Lett.*, vol. 44, no. 4, pp. 295-296, Feb., 2008.

[5] F. -C. Chen and Q. -X. Chu, "Compact Triple-Band Bandpass Filter Using Pseudointerdigital Trisection Stepped Impedance Resonators", *Microw. Opt. Technol. Lett.*, vol. 50, no. 9, pp. 2462-2465, Sept., 2008.

[6] Sun S.-J., Su Tao, Deng Kun, Wu Bian, and Liang C.-H, "Shorted-Ended Stepped-Impedance Dual-Resonance Resonator and Its Application to Bandpass Filters", *IEEE Trans. Microw. Theory Tech.*, vol. 61, no. 9, pp. 3209-3215, Sept., 2013.

[7] Jun Li, Shan Shan Huang, Hui Wang, and Jian Zhong Zhao, "Compact Dual-Band Bandpass Filter Using Embedded Center-Grounded SIR and Open-Loop Resonators", *Progr. Electromagn. Res. Lett.*, vol. 49, pp. 9-14, Sep., 2014.

[8] Jun Li, Shan Shan Huang, and Jian Zhong Zhao, "Design of a Compact and High Selectivity Tri-Band Bandpass Filter Using Asymmetric Stepped-Impedance Resonators (SIRs)", *Progr. Electromagn. Res. Lett.*, vol. 44, 81-86, Jan., 2014.

[9] H-W. Wu and R-Y. Yang, "Design of a Triple-Passband Microstrip Bandpass Filter With Compact Size", *J. Electromagn. Waves Appl.*, vol. 24, no. 17-18, pp. 2333-2341, 2010.

[10] Liu, S-K., and F-Z. Zheng, "A New Compact Tri-Band Bandpass Filter Using Step Impedance Resonators With Open Stubs", *J. Electromagn. Waves Appl.*, vol. 26, no. 1, pp. 130-139, 2012.

[11] Chen Wei-Yu, Min-Hang Weng, and Shoou-Jinn Chang, "A New Tri-Band Bandpass Filter Based on Stub-Loaded Step-Impedance Resonator", *IEEE Microw. Wireless Compon. Lett.*, vol. 22, no. 4, pp. 179-181, Apr., 2012.

[12] K. Xu, Y. Zhang, D. Li, Y. Fan, J. L.-W. Li, W. T. Joines, and Q. H. Liu, "Novel Design of a Compact Triple-Band Bandpass Filter Using Short Stub-Loaded SIRs and Embedded SIRs Structure", *Progr. Electromagn. Res.*, vol. 142, pp. 309-320, 2013.

[13] Chen, J-Z., et al, "Fourth-Order Tri-Band Bandpass Filter Using Square Ring Loaded Resonators", *Electron. Lett.*, vol. 47, no. 15, pp. 858-859, 2011.

[14] Doan M. T., W. Q. Che, and W. J. Feng, "Tri-Band Bandpass Filter Using Square Ring Short Stub Loaded Resonators", *Electron. Lett.*, vol. 48, no. 2, pp. 106-107, 2012.

[15] S. J. Sun, L. Lin, B. Wu, K. Deng, and C.-H. Liang, "A Novel Quad-Mode Resonator and Its Application to Dual-Band Bandpass Filters", *Progr. Electromagn. Res. Lett.*, vol. 43, pp. 95-104, 2013.

[16] Xu J., Miao C., Cui L., Ji Y.-X., and Wu W, "Compact High Isolation Quad-Band Bandpass Filter Using Quad-Mode Resonator", *Electron. Lett.*, vol. 48, no. 1, pp. 28-30, 2012.

[17] Jun Li, Shan Shan Huang, and Jian Zhong Zhao, "Compact Microstrip Dual-Wideband Bandpass Filter Using a Novel Multi-Mode Resonator", *Open Science Journal of Electrical and Electronic Engineering*, to be published, 2014.

[18] Gao Li, and Xiu Yin Zhang, "High-Selectivity Dual-Band Bandpass Filter Using a Quad-Mode Resonator With Source-Load Coupling", *IEEE Microw. Wireless Compon. Lett.*, vol. 23, no. 9, pp. 474-476, Sept., 2013.

[19] Jun Li, Shan-Shan Huang, and Jian-Zhong Zhao, "Compact Dual-Wideband Bandpass Filter Using a Novel Penta-Mode Resonator (PMR)", *IEEE Microw. Wireless Compon. Lett.*, vol. 24, no. 10, pp. 668-670, Oct., 2014.

[20] Gómez-García Roberto, and José I. Alonso, "Design of Sharp-Rejection and Low-Loss Wide-Band Planar Filters Using Signal-Interference Techniques", *IEEE Microw. Wireless Compon. Lett.*, vol. 15, no. 8, pp. 530-532, Aug., 2005.